Structures of Quenched $Li_xMn_{3-x}O_4$ Spinels

Paweł Piszora*

Laboratory of Magnetochemistry, Adam Mickiewicz University, Grunwaldzka 6, PL-60780 Poznań, Poland

Received April 27, 2006. Revised Manuscript Received July 5, 2006

The pseudo-ternary Li−Mn−O phase diagram at 20 °C has been extended by three new phases. The lithium-deficient orthorhombic phase (*Fddd*), isostructural with low-temperature $LiMn_2O_4$, has for the first time been obtained by the steering of manganese occupancy and valence on tetrahedral sites. The influence of lithium deficiency on the formation of various crystal structures is shown, accompanied by their structural parameters resulting from the Rietveld refinement. Valence of manganese at tetrahedral sites has been proven as playing a key role in the phase transitions of the lithium-deficient lithium−manganese oxides.

Introduction

Temperature phase transitions of lithium−manganese spinel have been studied very intensively in the past decade. Yamada and Tanaka[1] have reported the phase transition at a temperature close to room temperature, and since that moment the low-temperature phase has been examined very intensively. Although primarily the room temperature (RT) phase transition had been described as cubic → tetragonal. More precise structural investigations have proved that it is a transition from cubic ($Fd\bar{3}m$) to orthorhombic (*Fddd*), and the orthorhombic unit-cell is nine times bigger than the cubic one due to the superstructure.[2] This phase transition has been considered as one of the reasons for capacity fading of batteries built with $LiMn_2O_4$ as an anode material. While the RT phase transition has been well-established, the additional orthorhombic → tetragonal phase transition in the temperature region of 60−100 K has been reported.[3] Finally, with the application of very fine experimental resolution of measurements, $LiMn_2O_4$ at a temperature of 10 K has been unambiguously identified as orthorhombic.[4] Doping of $LiMn_2O_4$ with various metals (e.g., Co, Fe, Cr, Ni, Li) has been revealed as a simple method of suppressing the RT phase transition.[5] The temperature of phase transition can be decreased by doping, and finally, for a sufficient amount of dopant, the cubic phase is preserved down at 10 K. Nevertheless, for an intermediate composition (e.g., $Li_{1.025}Mn_{1.975}O_4$) the phase transition seems to be cubic → tetragonal rather than cubic → orthorhombic.[6]

Parallel to low temperature investigations, the structure of lithium−manganese oxides at high temperatures has been investigated, but unfortunately with high divergence of results. For comprehensive comparison, see ref 7. Broadly speaking, $LiMn_2O_4$ has proven to be thermally unstable and during heating usually has decomposed to $Li_xMn_{3-x}O_4$ and additional oxides. At as a low temperature as 450 °C, the thermal decomposition can be observed. This decomposition leads to the spinel phase, with the most probable formula of $LiMn_{2-\epsilon}O_4$, where the manganese valence is >3.5, and to Mn_2O_3 as an additional phase.[7] Further heating results in the solid-state reaction between the spinel and the nonspinel phases, creating $LiMn_2O_4$ again.

While the temperature of phase transition in lithium−manganese oxide depends strictly on the cation distribution and on the valence of manganese, the key to understanding the appearance and the nature of phase transition is the detailed knowledge about sample preparation and measurement conditions. The sintering process at a temperature of 300−700 °C and/or height partial pressure of oxygen direct the synthesis to products with the average oxidation state of Mn higher than in stoichiometric $Li^+Mn_2^{+3.5}O_4$ and, as a consequence, depress an RT phase transition. At temperatures above 800 °C one can observe the existence of $Li_xMn_{3-x}O_4$ with the Mn valence <3.5 and some additional lithium−manganese oxides. Thackeray et al.[8] have studied the thermal stability of $LiMn_2O_4$. They have observed, at a temperature range of 1113−1273 K, the lithium-rich Li_2MnO_3 phase in addition to the lithium-deficient lithium−manganese spinel. The high-temperature spinel structure has been described as tetragonal with space group $F4_1/ddm$ and a distortion $c/a > 1$ ($c/a = 1.02$ at 1073 K). At the temperature above 1233 K, the nonspinel $LiMnO_2$ oxide, with manganese 3+, has replaced Li_2MnO_3, with manganese 4+. Above 1393 K the $LiMnO_2$ phase has been reincorporated into a hausmannite-like lithium manganese spinel considered as the solid solution between $Li^+Mn_2^{+3.5}O_4$ and $Mn_3^{+2.67}O_4$.

Many papers have treated of samples quenched during sintering and subsequently examined in ambient condition

* To whom correspondence should be addressed. Phone: +48618291262. Fax: +48618658008. E-mail: pawel@amu.edu.pl.

(1) Yamada, A.; Tanaka, M. *Mater. Res. Bull.* **1995**, *30*, 715.
(2) Rodríguez-Carvajal, J.; Rousse, G.; Masquelier, C.; Hervieu, M. *Phys. Rev. Lett.* **1998**, *81*, 4660.
(3) Piszora, P.; Darul, J.; Nowicki, W.; Wolska, E. *J. Alloys Compd.* **2004**, *362*, 231.
(4) Piszora, P.; Paszkowicz, W.; Baehtz, C.; Wolska, E. *J. Alloys Compd.* **2004**, *382*, 119.
(5) Molenda, J.; Marzec, J.; Świerczek, K.; Pałubiak, D.; Ojczyk, W.; Ziemnicki, M. *Solid State Ionics* **2004**, *175*, 297.
(6) Wolska, E.; Piszora, P.; Darul, J.; Nowicki, W. *J. Phys. Chem. Solids* **2004**, *65*, 223.
(7) Strobel, P.; Rousse, G.; Ibara-Palos, A.; Masquelier, C. *J. Solid State Chem.* **2004**, *177*, 1.
(8) Thackeray, M. M.; Mansuetto, M. F.; Dees, D. W.; Vissers, D. R. *Mater. Res. Bull.* **1996**, *31*, 133.

10.1021/cm0609855 CCC: $33.50
Published on Web 09/01/2006

as "high-temperature samples". As has been proven recently,[9] the high-temperature structure and the structure of the quenched sample are not always adequate.

A deformation of the spinel unit-cell was attributed to the Jahn−Teller distortion. The stoichiometric compound, $LiMn_2O_4$, presents a first-order phase transition close to room temperature, but temperature is not the only factor affecting structural changes. The most recent researches show structural phase transition as a result of pressure.[10,11]

One more reason for structural changes in the lithium−manganese spinel is modulation of the chemical composition. Even a small deficit of lithium can dramatically involve essential changes in the crystal structure. Appearance of unit-cell deformation depends on the average manganese valence in octahedral sites, particularly on the molar ratio of Mn^{3+} ions. The average manganese valence in stoichiometric $LiMn_2O_4$ is 3.5. Raising of this value (e.g., by doping) stabilizes the cubic structure even below RT. Decreasing of Mn valence leads to the cooperative Jahn−Teller effect and lowers the symmetry of crystals. These non-cubic structures can be observed in lithium-deficient samples.

Experimental Section

The series of $Li_xMn_{3-x}O_4$ ($0.85 \leq x \leq 1.00$) sample was obtained by combining the sol−gel auto-combustion method and the ceramic method. The detailed process can be described as follows. The titrated solution of $Mn(NO_3)_2 \cdot 6H_2O$ (99.0% Merck) and the equimolar solution of $C_6H_8O_7 \cdot H_2O$ were used as raw materials. An aqueous ammonia solution was slowly added to adjust the pH to ~7. Then, the stabilized nitrate−citrate sol was poured into a porcelain evaporating dish and slowly heated. Viscosity and color changed as the sol turned into a puffy, porous dry gel. If ignited, the dried gel burned completely to a loose powder. Subsequently, the powder sample was annealed for 2 h at 873 K to obtaine a crystalline single-phase precursor displaying the bixbyite (*Ia*3) structure. The spinel sample was obtained from Li_2CO_3 (Merck) and α-Mn_2O_3 powders, by a solid-state reaction in air at 1043 K for 4 h. Finally the sample was quenched rapidly in the solid CO_2. An inductively coupled plasma emission spectrophotometer (ICP) was used to confirm the sample composition.

Structural investigations were carried out at the synchrotron beam-line I711 at MAX-Lab with an image foil Huber 670 Guiner camera,[12] with a Cryostream cooler (Oxford Cryosystem) and with a furnace for the Huber detector in the high-temperature measurements. The wavelength, $\lambda = 1.2722$ Å, was determined by calibration using NIST silicon standard. The data analysis was performed with GSAS software[13] with the graphical user interface EXPGUI.[14]

Results

X-ray powder diffraction data collected at room temperature on series of lithium-deficient samples were analyzed by the Rietveld method (Figure 1). The pseudo-Voigt function for peak profiles was used with coefficients as parametrized by Thompson et a1.,[15] asymmetry correction of Finger et a1.,[16] and anisotropic peak broadening of Stephens.[17] Observed anisotropic microstrain distributions may be caused by composition distributions of the quenched samples. For background fitting, a shifted Chebyshev function was used.

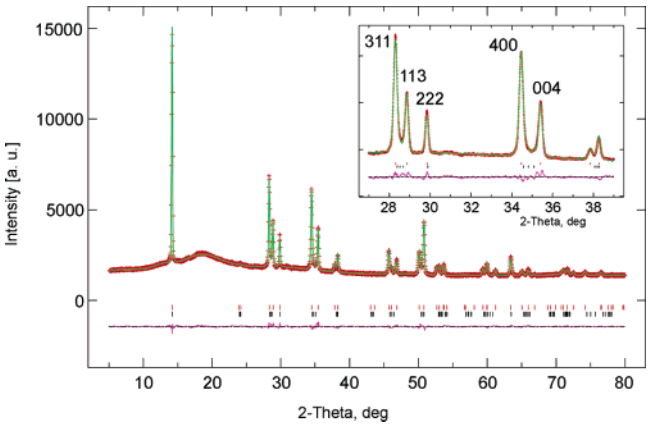

Figure 1. Observed, calculated, and difference profiles resulting from the Rietveld analysis of X-ray powder diffraction. Data collected on $Li_{0.94}Mn_{2.06}O_4$.

Phase Analysis. Collected XRD patterns (Figure 2) can be grouped into four sets with different structures of the major phase:

I. In the region of Li content between 1.00 and 0.98 practically the only crystal phase is the cubic phase with the space group $Fd\bar{3}m$. Only small traces of the additional tetragonal phase can be noticed in the pattern of $Li_{0.98}Mn_{2.02}O_4$; nevertheless, for this sample the additional orthorhombic phase considered during refinement significantly improved the R factors.

II. Samples with composition from $Li_{0.97}Mn_{2.03}O_4$ to $Li_{0.94}Mn_{2.06}O_4$ reveal the tetragonal "flattened" structure with $c/a < 1$ and space group $F4_1/ddm$. The nonstandard face-centered space group was selected instead of $I4_1/amd$ to better show the spinel structure deformation. The observable amount of the additional orthorhombic phase decreases in this region with the decrease of lithium content (Figure 3).

Two possible explanations of coexistence of the tetragonal phase and of the orthorhombic phase, analogous to the low-temperature polymorph of $LiMn_2O_4$, could be taken into considerations. The first is a temperature gradient inside the sample during quenching process, which can results in small differences in local composition and adequate structural deformations. The other reason could be a disproportionation to the energetically more stable phases. Anyhow, improvement of the crystal homogeneity is essential and needs more studies.

III. In the XRD pattern of sample with nominal composition $Li_{0.93}Mn_{2.07}O_4$ the main phase can be identified as orthorhombic with space group *Fddd*. Two minor phases can be both indexed with the tetragonal $F4_1/ddm$ space group

(9) Piszora, P. *J. Alloys Compd.* **2005**, *401*, 34.
(10) Piszora, P.; Paszkowicz, W.; Nowicki, W.; Minikayev, R.; Lathe, C. *HASYLAB Annual Report*; 2003; p 309.
(11) Paolone, A.; Sacchetti, A.; Postorino, P.; Cantelli, R.; Congeduti, A.; Rousse, G.; Masquelier, C. *Solid State Ionics* **2005**, *176*, 635.
(12) Ståhl, K. *J. Appl. Crystallogr.* **2000**, *33*, 394.
(13) Larson, A. C.; Von Dreele, R. B. *Los Alamos National Laboratory Report LAUR*; 2000; p 86.
(14) Toby, B. H. *J. Appl. Crystallogr.* **2001**, *34*, 210.
(15) Thompson, P.; Cox, D. E.; Hastings, J. B. *J. Appl. Crystallogr.* **1987**, *20*, 79.
(16) Finger, L. W.; Cox, D. E.; Jephcoat, A. P. *J. Appl. Crystallogr.* **1994**, *27*, 892.
(17) Stephens, P. *J. Appl. Crystallogr.* **1999**, *32*, 281.

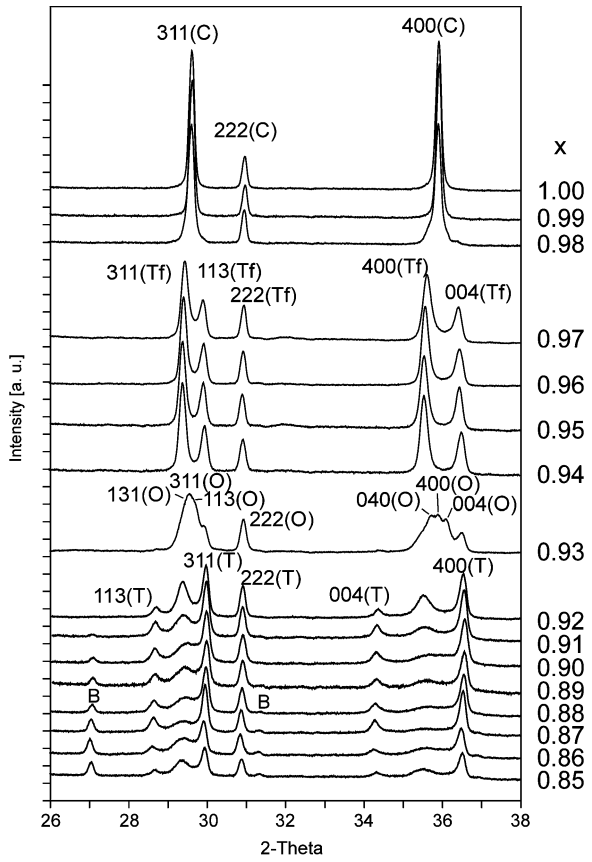

Figure 2. Section of X-ray diffraction pattern of $Li_xMn_{3-x}O_4$ in the range of cubic 311, 222, and 400 reflections.

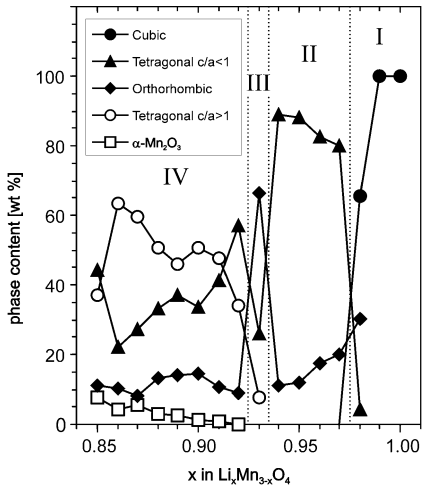

Figure 3. Phase composition in function of the nominal x in $Li_xMn_{3-x}O_4$.

but have different unit-cell ratios: $c/a < 1$ and $c/a > 1$. The superstructure reflections of the orthorhombic phase were very weak and very difficult to localize in this multiphase system, therefore "small" unit-cells (a, b, $c \cong 8$ Å) were applied.

IV. XRD patterns of samples with the nominal composition from $Li_{0.92}Mn_{2.08}O_4$ to $Li_{0.85}Mn_{2.15}O_4$ showed a significant amount of the crystal phase with the tetragonal structure (space-group $F4_1/ddm$) and the "elongated" unit-cell ($c/a > 1$). Beside the coexistence of tetragonal "flattened" and orthorhombic phases, for lithium content less than 0.92 the increasing amount of the bixbyite phase (α-Mn_2O_3) can be observed (Figure 3). Due to presence of this residual phase, determination of the real lithium content in the spinel phases could be only semiquantitative. It may be suspected that doping of $Li_xMn_{3-x}O_4$ (e.g., by zinc atoms) improve a crystalline phase purity. Result of our pretests for $Li_{0.93}Zn_{0.07}[Mn_2]O_4$ supported this theory.

Remarkable divergence between calculated and observed patterns is a consequence of the multiphase system with remarkable microstructure effects. Detailed profile fitting for each phase was not a simple task because of the significant microstructure effects and the strong peak overlapping. The multiphase character of samples can be a consequence of the quenching process and of the temperature gradient, limited by thermal conductivity of the sample, during its cooling. Despite very fast cooling (~1 s), the complex composition of the $Li_xMn_{3-x}O_4$ samples with x less than 0.93 can be attributed to the differences in the relaxation process (Figure 3).

An example of the Rietveld profile matching is presented in Figure 1. The inset shows a successful good fitting in the most representative 2Θ region (see Figure 2). The structural parameters obtained from the Rietveld refinement are given in Table 1. The manganese fractional occupancy refined for the tetrahedral site decreases in linear fashion with the lithium content, although this tendency is not so clear for $x < 0.93$ because of the complicated microstructure effects and the serious overlapping of reflection for the multiphase X-ray patterns.

Four compositional regions can be distinguished by means of the c/a axial ratio of the main crystal phase (Figure 4). The orthorhombic phase appears in the region III, separating the flattened tetragonal phase ($c/a < 1$) and the elongated tetragonal phase ($c/a > 1$). The c/a axial ratio of the elongated tetragonal phase corresponds well with $c/a = 1.06$ obtained for the $Li_{0.91}Mn_{2.09}O_4$ single-crystal grown by a flux method.[18]

Discussion

It is actually not possible to give an exact explanation of this sensitivity of the structure to a chemical composition. The main reason for the structural deformation, undoubtedly, is the Jahn−Teller effect in addition to changes in the orientation and displacement of non-spherical ions. Manganese migrates to the tetrahedral sites and, by the quenching process, the spinel phase can be stabilized. The following three models of the manganese ions distribution can be proposed.

Model A: $Li_xMn^{3+}_{1-x}[Mn^{3+}_{3-2x}Mn^{4+}_{2x-1}]O_4$. Rietveld refinement gives the fractional occupation of manganese ions at tetrahedral sites (Table 1); nevertheless, X-ray diffraction methods cannot distinguish between Mn^{2+} and Mn^{3+} ions. Comparison of the stabilization energy of those ions (Table 2) leads to the conclusion that the global energy minimum of this structure appears for Mn^{3+} ions at octahedral positions. However, the local energy minimum is possible if Mn^{3+} ions occupy tetrahedral sites. On the contrary, the Mn^{2+} ion does not prefer any position in the spinel structure, and it is moved

(18) Björk, H.; Dabkowska, H.; Greedan, J. E.; Gustafsson, T.; Thomas, J. O. *Acta Crystallogr. C* **2001**, *57*, 331.

Table 1. Unit-Cell Parameters, Unit-Cell Volume, Atomic Coordinates of the Oxygen Atom, and Fractional Occupancy of Lithium on Tetrahedral Sites Resulting from Rietveld Refinement of $Li_xMn_{3-x}O_4$[a]

nominal x in $Li_xMn_{3-x}O_4$	a, b [Å]	c [Å]	V [Å^3]	atomic coordinates of oxygen x	y	z	Li(tetr)
			Cubic $Fd\bar{3}m$				
1.00	8.249437(15)		561.4008(18)	0.26046(5)	0.26046(5)	0.26046(5)	0.964(1)
0.99	8.249567(17)		561.4272(20)	0.26084(6)	0.26084(6)	0.26084(6)	0.949(1)
0.98	8.252841(18)		562.096(2)	0.26232(7)	0.26232(7)	0.26232(7)	0.958(1)
			Tetragonal (c/a < 1) $F4_1/ddm$				
0.98	8.3181(3)	8.1427(5)	563.40(4)	−0.012036	0.012036	0.266291	0.9446
0.97	8.31623(5)	8.14246(7)	563.130(6)	−0.01116(9)	0.01116(9)	0.26223(12)	0.931(1)
0.96	8.33079(4)	8.13917(6)	564.876(5)	−0.01134(7)	0.01134(7)	0.26171(11)	0.921(1)
0.95	8.33539(4)	8.13808(6)	565.423(6)	−0.01119(8)	0.01119(8)	0.26235(12)	0.914(1)
0.94	8.33007(4)	8.12214(6)	563.596(6)	−0.01094(8)	0.01094(8)	0.26225(11)	0.902(1)
0.93	8.3402(3)	8.1391(4)	566.14(4)	−0.0048(5)	0.0048(5)	0.2748(7)	0.885
0.92	8.34571(10)	8.12564(15)	565.958(14)	−0.00900(19)	0.00900(19)	0.26600(27)	0.817(3)
0.91	8.35173(17)	8.1218(3)	566.51(3)	−0.0111(3)	0.0111(3)	0.2721(5)	0.826(4)
0.90	8.34422(21)	8.1167(3)	565.130(28)	−0.0167(4)	0.0167(4)	0.2753(6)	0.893(4)
0.89	8.3493(2)	8.1194(3)	566.00(3)	−0.0130(4)	0.0130(4)	0.2759(7)	0.826(5)
0.88	8.3516(2)	8.1174(4)	566.18(3)	−0.0134(4)	0.0134(4)	0.2751(7)	0.848(4)
0.87	8.3480(3)	8.1140(5)	565.46(4)	−0.0177(5)	0.0177(5)	0.2774(9)	0.856(5)
0.86	8.35215(19)	8.1223(3)	566.60(3)	−0.0121(4)	0.0121(4)	0.2772(6)	0.815(5)
0.85	8.34275(15)	8.1203(2)	565.18(2)	−0.0082(3)	0.0082(3)	0.2661(4)	0.861(4)
			Orthorhombic $Fddd$				
0.93	8.25888(16) 8.3043(2)	8.20918(14)	563.02(2)	0.7445(4)	0.7381(4)	0.74284(31)	0.845(5)
			Tetragonal (c/a > 1) $F4_1/ddm$				
0.93	8.1215(3)	8.5823(10)	566.08(7)	−0.0097(9)	0.0097(9)	0.2770(11)	0.885
0.92	8.11137(13)	8.6162(4)	566.90(3)	−0.0119(4)	0.0119(4)	0.2639(5)	0.845(3)
0.91	8.11302(11)	8.6236(3)	567.61(2)	−0.0080(3)	0.0080(3)	0.2584(4)	0.850(4)
0.90	8.10386(9)	8.6211(3)	566.172(19)	−0.0107(3)	0.0107(3)	0.2663(3)	0.918(4)
0.89	8.11056(13)	8.6267(4)	567.47(3)	−0.0074(4)	0.0074(4)	0.2601(4)	0.851(5)
0.88	8.11058(11)	8.6283(3)	567.59(2)	−0.0066(3)	0.0066(3)	0.2598(4)	0.873(4)
0.87	8.10933(11)	8.6208(3)	566.91(2)	−0.0072(3)	0.0072(3)	0.2602(4)	0.884(5)
0.86	8.11389(14)	8.6283(4)	568.04(3)	−0.0070(4)	0.0070(4)	0.2609(5)	0.840(5)
0.85	8.10853(14)	8.6110(4)	566.16(3)	−0.0085(5)	0.0085(5)	0.2633(5)	0.889(4)

[a] χ^2 from 0.4027 to 1.3410; Rwp from 1.66 to 2.79; Rp from 1.25 to 1.89. Values without standard deviation in parentheses were not refined. Atomic coordinates of tetrahedral Mn/Li: *Fddd*, $Fd\bar{3}m$ 0.125, 0.125, 0.125; $F4_1/ddm$ 0.875, 0.125, 0.875. Atomic coordinates of octahedral Mn: *Fddd*, $Fd\bar{3}m$ 0.5, 0.5, 0.5; $F4_1/ddm$ 0, 0, 0.5.

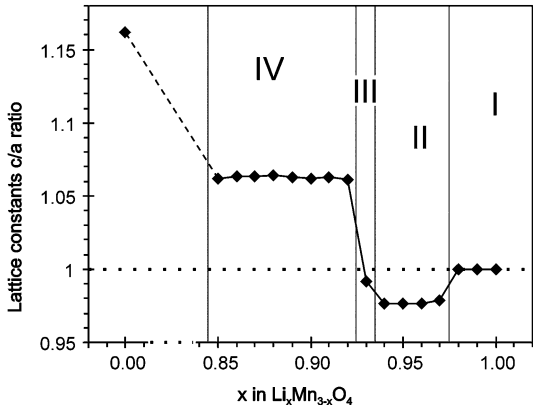

Figure 4. Axial ratio of the major crystal phases dependence of the lithium content.

Table 2. Comparison of Configuration, Field Distortion, and Stabilization Energy of Manganese Ions[a]

Configuration	Mn^{2+} d^5	Mn^{3+} d^4	Mn^{4+} d^3
Octahedral field	↑ ↑ ↑ ↑ ↑	↑ ↑ ↑ — —	— — — — —
Distortion		strong	
Es_{octa} [kJ/mol]	0	150.3*	285.5**
Tetrahedral field	↑ ↑ ↑ ↑ ↑	↑ ↑ — ↑ ↑	↑ — — ↑ ↑
Distortion		strong	strong
Es_{tetra} [kJ/mol]	0	44.4*	0

[a] *, according to ref 20; **, according to ref 21.

to the tetrahedral site if it occurs near Mn^{4+} and Mn^{3+} ions with the strong preference for octahedral sites. The Mn^{4+} ion does not move to tetrahedral sites because of its very strong stabilization in the octahedral crystal field.

The other problem is the ability of the $Li_xMn_{3-x}O_4$ spinel oxides to structurally deform. The Mn^{3+} ions elongate the octahedra in the spinel structure and leads (e.g., in Mn_3O_4) to an increase in the c unit-cell parameter. A more complicated orientation of elongated octahedra in the low-temperature $LiMn_2O_4$ can lead also to flattened structure with the c-axis shorter than a and b.

Mn^{3+} ions on tetrahedral sites can induce tetragonal deformation due to their asymmetric electron configuration (Table 2). The shortening of the c-axis and reducing of symmetry can be forced by the tetrahedrally coordinated Mn^{3+} ions.

Model B: $Li_xMn^{2+}_{1-x}[Mn^{3+}_{2-x}Mn^{4+}_x]O_4$. Interestingly, there is one more competitive scenario of the constraint of phase transition. Due to high stabilization of the Mn^{4+} ion in the octahedral field, the crystal can be stabilized by reduction of manganese in the tetrahedral position to Mn^{2+} and by increasing the amount of Mn^{4+} in the octahedral position. This disproportionation suppresses the distortion of the tetrahedron and leads to the tetragonally elongated spinel

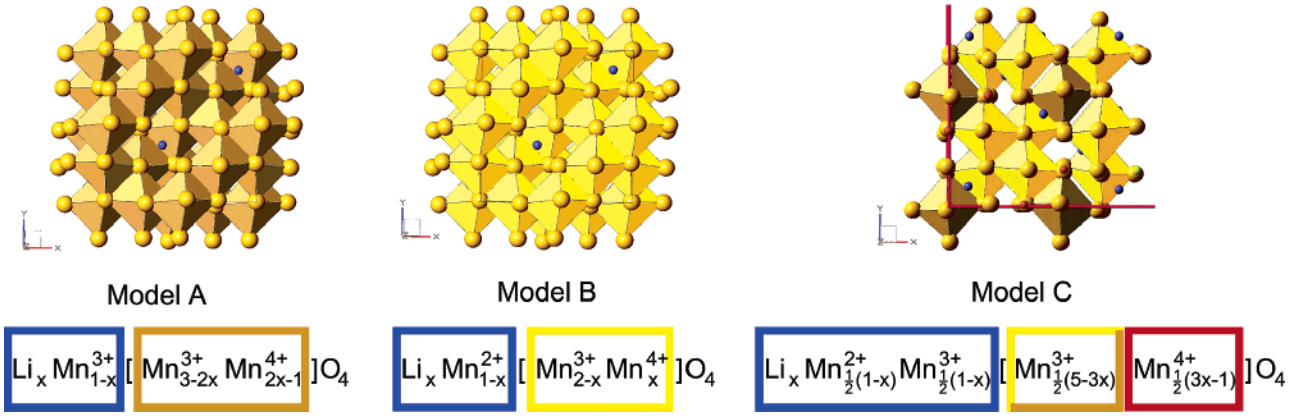

Figure 5. Cation distribution over tetrahedral and octahedral spinel sites in three proposed models: brown, the octahedra elongated in *z* direction; yellow, the elongated octahedra oriented in *x* or *y* direction. In model C, only $Mn^{3+}O_6$ are shown as octahedra, and 1/9th of the orthorhombic unit-cell is represented graphically as compared with models A and B.

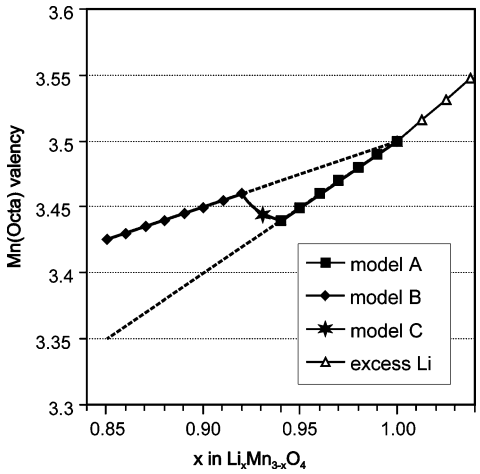

Figure 6. Calculated average valence of octahedral surrounding manganese: square, Mn^{3+} at tetrahedral sites (model A); diamond, Mn^{2+} at tetrahedral sites (model B); asterisk, 1:1 Mn^{3+} and Mn^{2+} mixture at tetrahedral sites (model C). For further description, see text.

structure, because even in this case the average oxidation state of manganese at octahedral sites is less than 3.5.

Therefore the presence of Mn^{3+} ions on tetrahedral sites can force the elongated octahedrons to an orientation parallel to the *xy* plane (tetragonally flattened spinel structure), model A; whereas in the structure with Mn^{2+} ions on tetrahedral sites the $Mn^{3+}O_6$ octahedrons are oriented to the *z* direction (as in the hausmannite structure), model B (Figure 5).

Model C: $Li_xMn^{2+}_{\frac{1}{2}(1-x)} Mn^{3+}_{\frac{1}{2}(1-x)}[Mn^{3+}_{\frac{1}{2}(5-3x)} Mn^{4+}_{\frac{1}{2}(3x-1)}]O_4$. The orthorhombic structure (space group *Fddd*) of the low-temperature $LiMn_2O_4$ has five different octahedral positions with partially ordered Mn^{3+} and Mn^{4+} ions.[2] It is impossible to order an equimolar amount of Mn^{3+} and Mn^{4+} ions on five crystallographic positions. Nevertheless, if we assume that the orthorhombic structure as the intermediate one between the flattened tetragonal structure and the elongated tetragonal structure, we can suspect a manganese valence of about 2.5 on tetrahedral sites, model C. For such mixed valence and the $Li_{0.93}Mn_{2.07}O_4$ stoichiometry, the average calculated valence is 3.4475 and is very close to 3.4444 calculated for a completely ordered orthorhombic structure (Mn^{3+} as Mn(1), Mn(2), and Mn(3); Mn^{4+} as Mn(4) and Mn(5)[2]) (Figure 6).

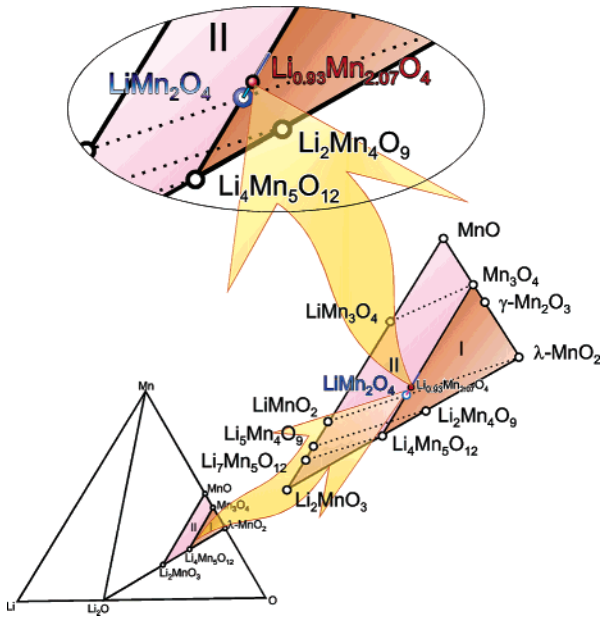

Figure 7. Li−Mn−O phase diagram with an expanded region of examined $Li_xMn_{3-x}O_4$ samples and pointed orthorhombic $Li_{0.93}Mn_{2.07}O_4$.

To the author's knowledge this is the first time that a lithium−manganese spinel with completely columnary ordering of charge has been observed. The presented results open up new vistas of the controlled electronic crystallization in spinel-type oxides. The intentional modification of the manganese valence state at each of the crystallographic positions in the orthorhombic $Li_xMn_{3-x}O_4$ can lead to the creation of new sorts of semiconducting materials. Nevertheless, the sintering conditions need to be improve to obtain a single phase sample.

The structure of the $Li_xMn_{3-x}O_4$ samples obtained by the quenching process used to be identified as a high-temperature structure. Nevertheless, at a high final annealing temperature (about 1173 K[9] or 1253 K[19]), the lithium-deficient lithium−manganese oxide retains the cubic structure ($Fd\bar{3}m$). Despite the above, surprisingly, the quenching procedures lead to a lowering of the crystal symmetry. Both the *a* unit-cell

(19) Massarotti, V.; Capsoni, D.; Bini, M. *Solid State Commun.* **2002**, *122*, 317.
(20) McClure, D. S. *J. Phys. Chem. Solids* **1957**, *20*, 311.
(21) Dittman, R. Z. *Physica* **1968**, *216*, 183.

parameter and the fractional manganese occupancy at the tetrahedral sites start to increase rapidly above the temperature of 1045 K.[9] This temperature value was estimated as an optimal synthesis temperature.

Concerning the differences between the structure before and after the quenching process and taking into account the results of Rietveld refinement, the two tetragonal and one orthorhombic structure presented, can be located on the isothermal cross section of the Li−Mn−O phase diagram at 20 °C (Figure 7). They lie on the tie line between Mn_3O_4 and $Li_4Mn_5O_{12}$, consisting of spinel type structures with fully occupied anionic and cationic sites. This line separates the areas I and II which represent regions of defect spinel and defect rock salt structure, respectively.

Summary and Conclusions

The lithium deficient samples, $Li_xMn_{3-x}O_4$, with as small compositional step as $x = 0.01$ have been prepared in a range of $1 \geq x \geq 0.85$. The detailed phase analyses in this compositional region reveal the existence of three distorted spinel phases: two tetragonal phases with the different c/a axial ratio, both indexed with space group $F4_1/ddm$, and one orthorhombic phase with space group *Fddd*. It is the first time the existence of the orthorhombic phase even above RT has been proved as the intermediate structure between the tetragonally flattened spinel structure ($c/a < 1$) and the tetragonally elongated spinel structure ($c/a > 1$). The explanation of phase variation in the lithium-deficient manganese spinel series has been presented based on the lithium content on tetrahedral sites and the valence of manganese ions on both tetrahedral and octahedral sites. The amount of tetrahedrally coordinated Mn^{2+} and Mn^{3+} ions seems to play a key role in the structural preferences of lithium-deficient lithium−manganese spinel oxides.

Acknowledgment. The author is grateful for the support of the European Community − Research Infrastructure Action under the FP6 "Structuring the European Research Area" Programme (through the Integrated Infrastructure Initiative "Integrating Activity on Synchrotron and Free Electron Laser Science"). The author also thanks Dr. Y. Cerenius (MAX-lab Lund) for assistance during the measurements.

CM0609855